Supplementary Information: Understanding Shape Selectivity Effects of Hydroisomerization using a Reaction Equilibrium Model

Shrinjay Sharma,[1] Marcello S. Rigutto,[2] Erik Zuidema,[2] Umang Agarwal,[2] Richard Baur,[2] David Dubbeldam,[3] and Thijs J.H. Vlugt[1]

[1)] *Engineering Thermodynamics, Process & Energy Department, Faculty of Mechanical Engineering, Delft University of Technology, Leeghwaterstraat 39, 2628CB Delft, The Netherlands*

[2)] *Shell Global Solutions International B.V., Amsterdam, The Netherlands*

[3)] *Van 't Hoff Institute of Molecular Sciences, University of Amsterdam, Science Park 904, 1098XH, Amsterdam, The Netherlands*

(*Electronic mail: t.j.h.vlugt@tudelft.nl)

The following items are presented in this Supplementary Information:

1. Force field parameters for alkanes.

2. Henry coefficients of C_8 isomers in different zeolites.

3. Selectivities of C_8 isomers relative to n-C_8 in the gas phase and different zeolites.

The following items are listed in the Supplementary Information (SI2.xlsx):

1. Chemical thermodynamic data for C_7 and C_8 isomers obtained from tables by Scott[1].

2. Gas phase distribution of C_7 isomers at infinite dilution.

3. Gas phase distribution of C_8 isomers at infinite dilution.

4. Adsorbed phase distribution of C_7 isomers at infinite dilution.

5. Adsorbed phase distribution of C_8 isomers at infinite dilution.

6. Critical temperatures, critical pressures, and acentric factors of C_7 isomers.

7. Pure component fugacities and fugacity coefficients of C_7 isomers.

8. Gas phase distribution of C_7 isomers at finite loadings.

S1. FORCE FIELD PARAMETERS FOR ALKANES

TABLE S1: Lennard-Jones force field parameters for united atoms to account for intramolecular and intermolecular non-bonded interactions in alkanes. These parameters are taken from Dubbeldam *et al*[2].

united atom	ε/k_B/ [K]	σ/ [Å]
CH_3	108.0	3.76
CH_2	56.0	3.96
CH	17.0	4.67
C	0.8	6.38

TABLE S2: Lennard-Jones force field parameters for zeolite atoms to account for intermolecular non-bonded interactions between zeolite atoms and alkanes. These parameters are taken from Bai *et al*[3].

atom	ε/k_B/ [K]	σ/ [Å]
O	53.0	3.30
Si	22.0	2.30

Table S1 lists the Lennard-Jones parameters for the united atoms present in alkanes. These parameters are used to compute intramolecular and intermolecular interactions of alkane chains and are taken from Dubbeldam *et al*[2]. To account for the interactions between the zeolite atoms and alkane molecules, the TraPPE-zeo force field[3] is used. The Lennard-Jones parameters for O and Si are listed in Table S2. For interactions between different types of atoms, the Lennard-Jones parameters are calculated using the Lorentz-Berthelot mixing rules[4]. The TraPPE united atom force field is used for the intramolecular bonded interactions present in alkanes. These interactions are divided into bond-stretching, bond-bending, and torsion potentials. TraPPE force field uses a fixed $C-C$ bond length which is equal to 1.54 Å[3]. The bond-bending potential is described by a harmonic potential[5]:

$$U_{\text{bend}} = \frac{1}{2} k_{\text{bend}} (\theta - \theta_0)^2 \tag{S1}$$

TABLE S3: Values of the reference angles θ_0 and the force constants k_{bend} for different bend types.

bend type	θ_0/ [deg]	k_{bend}/k_B/ [K/rad^2]
$CH_x - CH_2 - CH_y$	114.0	62500
$CH_x - CH - CH_y$	112.0	62500
$CH_x - C - CH_y$	109.47	62500

TABLE S4: Values of the coefficients in the TraPPE united atom torsion potential[6] for different torsion types.

torsion type	c_0/k_B/ [K]	c_1/k_B/ [K]	c_2/k_B/ [K]	c_3/k_B/ [K]
CH_x-CH_2-CH_2-CH_y	0	355.03	-68.19	791.32
CH_x-CH_2-CH-CH_y	-251.06	428.73	-111.85	441.27
CH_x-CH_2-C-CH_y	0	0	0	461.29
CH_x-CH-CH-CH_y	-251.06	428.73	-111.85	441.27
CH_x-CH-C-CH_y	0	0	0	1635.7

In Eq. S1, k_{bend} is the force constant for the bending potential and θ is the bending angle. The values for the reference angles θ_0 are listed in Table S3[6]. These values depend on the type of united atom present at the center of the bend. The torsion potential is described by the three-cosine dihedral equation[5].

$$U_{\text{torsion}} = c_0 + c_1\left[1+\cos\left(\phi\right)\right] + c_2\left[1-\cos\left(2\phi\right)\right] + c_3\left[1+\cos\left(3\phi\right)\right] \tag{S2}$$

The coefficients (c_0, c_1, c_2, c_3) in Eq. S2 for different types of torsions are listed in Table S4[6]. Table S4 lists the values of the coefficients for different torsions described by the three-cosine dihedral equation. The TraPPE force field[6] parameters for the torsion type CH_x-C-C-CH_y are not available. In this study, this torsion type is described by a six-cosine dihedral equation (Eq. S3)[2]. The values of the coefficients, η_n are obtained from Dubbeldam *et al*[2] as listed in table S5.

$$U_{\text{torsion}} = \sum_{n=0}^{5} \eta_n \cos^n\left(\phi\right) \tag{S3}$$

TABLE S5: Values of the coefficients in the torsion potential for the CH_x-C-C-CH_y-torsion type (Eq. S3).

torsion type	η_0/k_B/ [K]	η_1/k_B/ [K]	η_2/k_B/ [K]	η_3/k_B/ [K]	η_4/k_B/ [K]	η_5/k_B/ [K]
CH_x-C-C-CH_y	2045.66	6136.80	0	-8182.45	0	0

S2. HENRY COEFFICIENTS OF C_8 ISOMERS IN DIFFERENT ZEOLITES

Figs. S1-S2 show the variations in Henry coefficients for C_8 isomers in FAU- and ITQ-29-type zeolites. FAU- and ITQ-29-type zeolites favor multi-branched isomers over mono-branched isomers. These variations are less significant in FAU-type zeolite because of the larger channel diameters $\left(7.4\ \text{Å}\right)$[7] which connects the cage-type pores.

Figs. S3-S5 show the variations in the Henry coefficients for different C_8 isomers in BEA-, MEL-, and MFI-type zeolites. BEA- and MEL-type zeolites show similar trends in Henry coefficients for mono- and di-branched isomers, which decrease with increasing degree of branching in both zeolites. For the mono-branched isomers, 3eC_6 has the least affinity for adsorption in both BEA- and MEL-type zeolites. 22mC_6, 33mC_6, and 3e3mC_5 have the smallest preference for adsorption compared to the other di-branched isomers. The tri-branched isomers have a lower affinity for adsorption in MEL-type zeolites compared to the di-branched isomers. This is because of the smaller pore diameters in MEL-type zeolite $\left(5.3 \times 5.4\ \text{Å}\right)$[7]. In MFI-type zeolite, 22mC_6 and 33mC_6 have larger Henry coefficients compared to other di-branched isomers. This is because the methyl branches can optimally fit into the intersections of MFI-type zeolite. As the separation distance between the methyl groups increases (24mC_6 versus 25mC_6), the likelihood for either branch attempting to fit into the channel-like pores increases, which is not favored in MFI-type zeolite. The tri-branched and the tetra-branched isomers are the least favored isomers in MFI-type zeolite due to the smaller pore diameters $\left(\text{sinusoidal channels} : 5.1 \times 5.5\ \text{Å and straight channels} : 5.3 \times 5.6\ \text{Å}\right)$[7] which leads to steric hindrance in presence of multiple branches in close proximity.

Fig. S6 shows the Henry coefficients for C_8 isomers in MTW-type zeolite. Similar to C_7 isomers, an overall decrease in the Henry coefficients with increasing degree of branching is observed for C_8 isomers. The presence of two methyl groups or a combination of a methyl and an ethyl group does not favor the adsorption of 22mC_6, 33mC_6, 3e2mC_5, and 3e3mC_5 in the

one-dimensional pores of MTW-type zeolite. MRE-type zeolite also shows a decrease in Henry coefficients as the degree of branching increases (Fig. S7). There is a sharp decrease in the Henry coefficients compared to those in MTW-type zeolite. This is because MRE-type zeolite has comparatively smaller channel diameters $\left(5.6 \times 5.6 \text{ Å}\right)$ than MTW-type zeolite $\left(6.0 \times 5.6 \text{ Å}\right)$[7]. The presence of an ethyl group does not favor the adsorption of 3e2mC_5 and 3e3mC_5 isomers in the MRE-type zeolite. Two branches attached to the adjacent carbon atoms in the main chain is not preferred in MRE-type zeolites. This can be attributed to the corrugations present inside the channels. Typical snapshots of MRE-type zeolite are shown in the main text in Section 4 (Fig. 8 of the main text). These corrugations are periodic combinations of peaks and crests which leads to variations in diameter inside the channels. The effects of corrugations can be quantified using the pore bumpiness factor[8]. This factor is defined as the difference between the maximum diameter of a sphere that can be included inside the channel and the maximum diameter of a sphere that can freely diffuse inside the channel[8]. The bumpiness factor for MRE-type zeolite is 0.77 Å. When two branches are adjacent to each other in the isomers, one of these have a higher probability to be fitted in the region of smaller channel diameter. This explains why in addition to 3e2mC_5, the molecules 23mC_6 and 34mC_6 also have comparatively lower Henry coefficients.

S3. SELECTIVITIES OF C_8 ISOMERS RELATIVE TO n-C_8 IN THE GAS PHASE AND DIFFERENT ZEOLITES

Selectivities in the gas phase and the adsorbed phase are defined as the ratio of the mole fraction of a component to the sum of the mole fractions of all other components present in the same phase[9]:

$$s_i^{\text{gas}} = \frac{y_i}{\left(\sum_{n=1}^{N} y_n\right) - y_i} \tag{S4}$$

$$s_i^{\text{ads}} = \frac{x_i}{\left(\sum_{n=1}^{N} x_n\right) - x_i} \tag{S5}$$

In Eq. S4, y_i is the mole fraction of component i in the gas phase. x_i is the mole fraction of component i in the adsorbed phase (Eq. S5). Selectivities of isomers relative to a reference molecule in the gas phase $\left(s_{\text{rel},i}^{\text{gas}}\right)$ and adsorbed phase $\left(s_{\text{rel},i}^{\text{ads}}\right)$ are defined as:

$$s_{\mathrm{rel},i}^{\mathrm{gas}} = \frac{s_i^{\mathrm{gas}}}{s_{\mathrm{ref}}^{\mathrm{gas}}} = \frac{\frac{y_i}{\left(\sum_{n=1}^{N} y_n\right) - y_i}}{\frac{y_{\mathrm{ref}}}{\left(\sum_{n=1}^{N} y_n\right) - y_{\mathrm{ref}}}} \tag{S6}$$

$$s_{\mathrm{rel},i}^{\mathrm{ads}} = \frac{s_i^{\mathrm{ads}}}{s_{\mathrm{ref}}^{\mathrm{ads}}} = \frac{\frac{x_i}{\left(\sum_{n=1}^{N} x_n\right) - x_i}}{\frac{x_{\mathrm{ref}}}{\left(\sum_{n=1}^{N} x_n\right) - x_{\mathrm{ref}}}} \tag{S7}$$

In Eqs. S6 and S7, y_{ref} and x_{ref} are the mole fractions of the reference molecule in the gas phase and adsorbed phase. In this case, n-C_8 is the reference molecule. Fig. S8 shows the selectivities of C_8 isomers relative to n-C_8 at reaction equilibrium in the gas phase. n-C_8 and the mono-branched isomers exhibit little variations in the magnitudes of selectivities. 3e2mC_5 and 3e3mC_5 isomers have the smallest selectivities compared to other di-branched isomers. 2233mC_4 is the least preferred isomer compared to all C_8 isomers. These observed trends in the selectivities at reaction equilibrium in the gas phase solely rely on the ratios of the isolated molecule partition functions of these isomers in the ideal gas phase.

Figs. S9-S15 show the selectivities of C_8 isomers relative to n-C_8 at reaction equilibrium in FAU-, ITQ-29-, BEA-, MEL-, MFI-, MTW-, and MRE-type zeolites. The variations in the selectivities are influenced by the combined effects of the isolated molecule partition functions in the gas phase and the Henry coefficients of these isomers in the zeolites. The influence of Henry coefficients on the reaction equilibrium distribution in the FAU-type zeolite is not very noticeable (Fig. S9). This is due to the presence of larger pore diameters $\left(7.4\ \text{Å}\right)$[7] in FAU-type zeolite. Multi-branched isomers preferentially adsorb in ITQ-29-type zeolite (Fig. S2). However, the variations in Henry coefficients are not very large in this zeolite. Therefore, the adsorbed phase distribution (Fig. S10) at reaction equilibrium closely resembles the gas phase distribution (Fig. S8). In BEA-, MEL-, and MFI-type zeolites, the mono-branched isomers are preferred at reaction equilibrium distribution. For zeolites with narrow channel-like pores such as MRE- and MTW-type zeolites, the variations in Henry coefficients are very important in deciding which isomers are preferentially formed at reaction equilibrium. MTW- and MRE-type zeolites prefer n-C_8 the most. In all zeolites considered in this study, 2233mC_4 is the least favored isomer at reaction equilibrium.

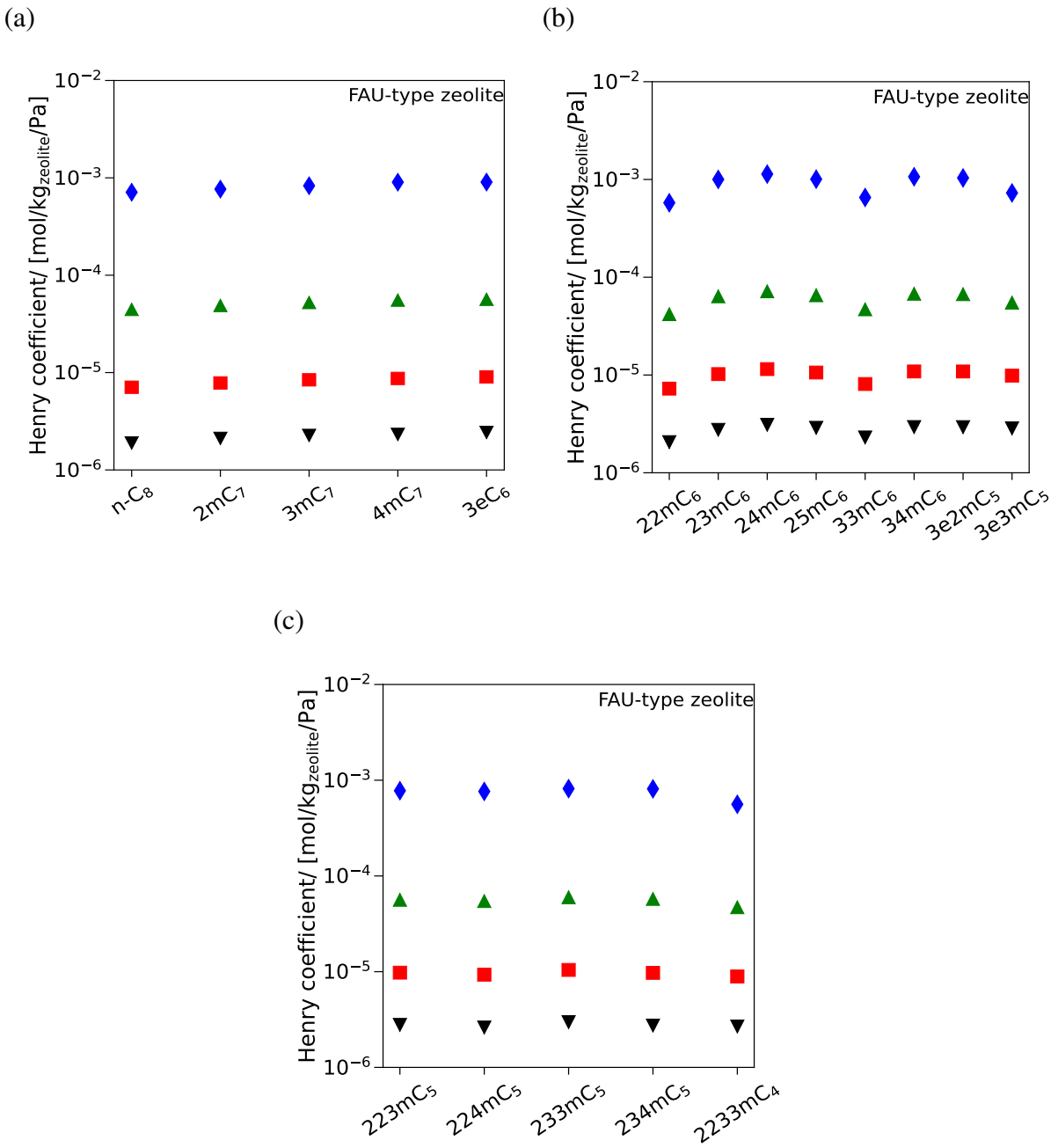

FIG. S1: Henry coefficients of C_8 isomers in FAU-type zeolite at ♦ 400 K, ▲ 500 K, ■ 600 K, and ▼ 700 K. The raw data is listed in the worksheets (xi_iC8_400K, xi_iC8_500K, xi_iC8_600K, and xi_iC8_700K) of the Supplementary Information (SI2.xlsx).

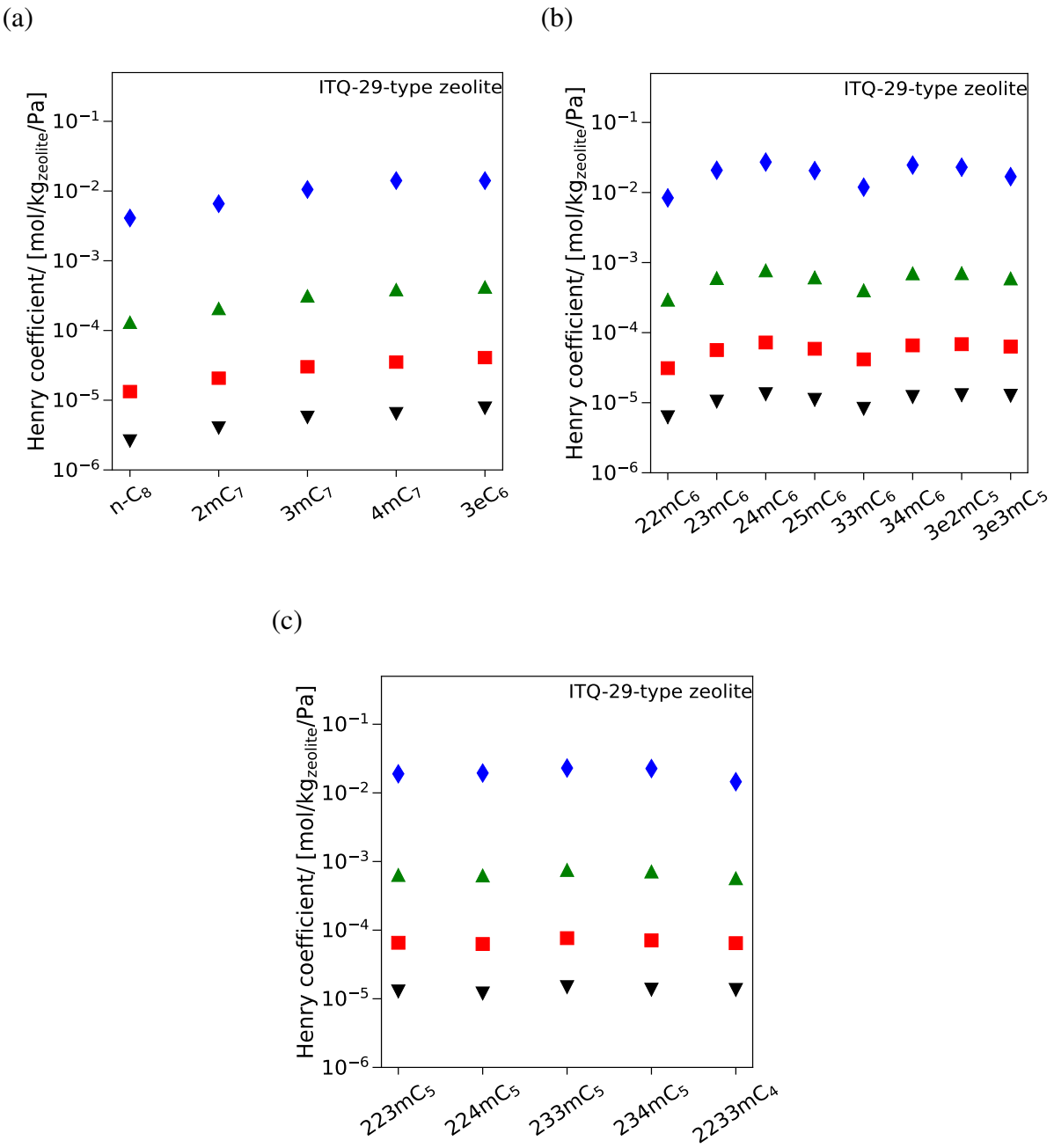

FIG. S2: Henry coefficients of C_8 isomers in ITQ-29-type zeolite at ♦ 400 K, ▲ 500 K, ■ 600 K, and ▼ 700 K. The raw data is listed in the worksheets (xi_iC8_400K, xi_iC8_500K, xi_iC8_600K, and xi_iC8_700K) of the Supplementary Information (SI2.xlsx).

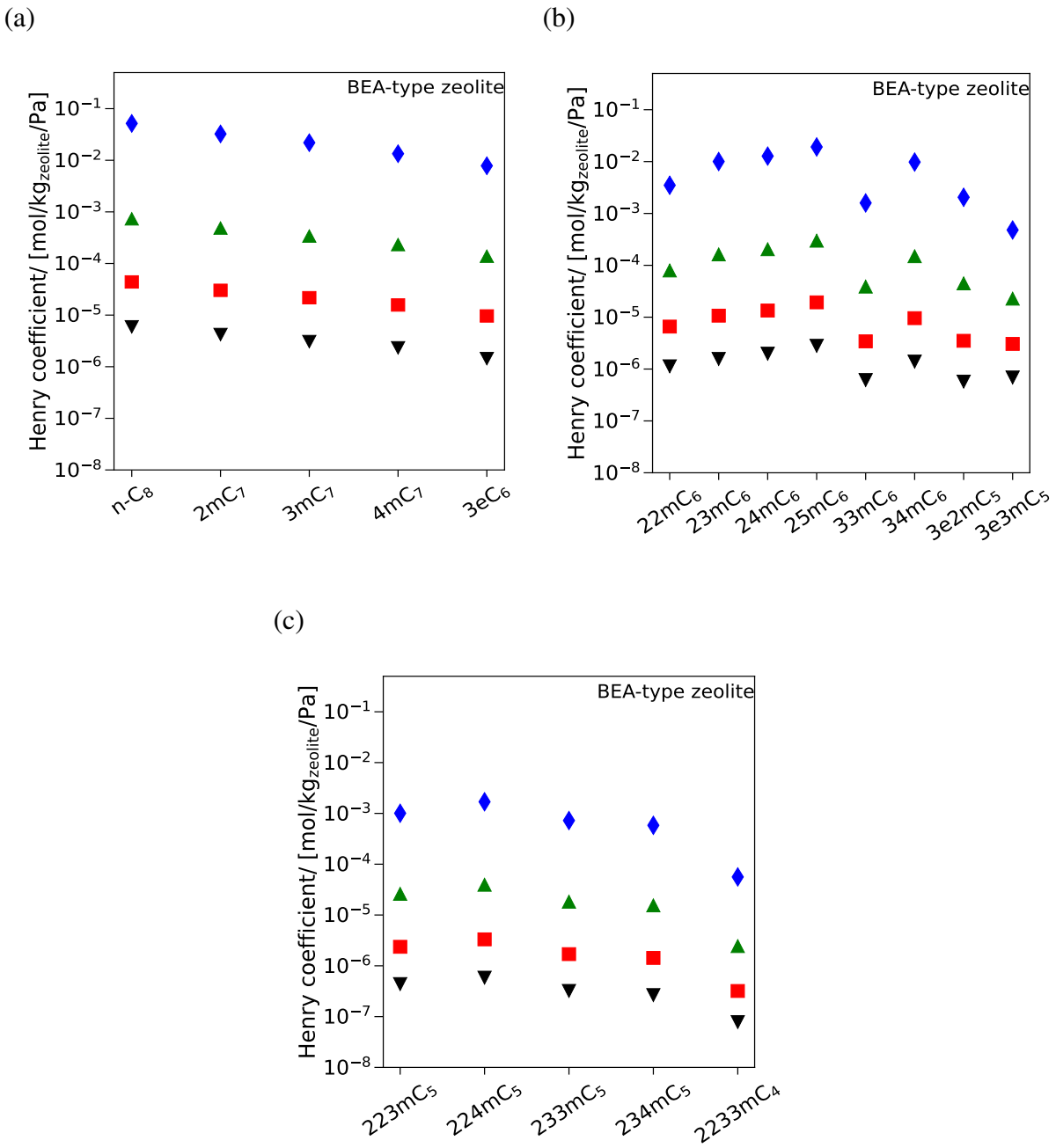

FIG. S3: Henry coefficients of C_8 isomers in BEA-type zeolite at ♦ 400 K, ▲ 500 K, ■ 600 K, and ▼ 700 K. The raw data is listed in the worksheets (xi_iC8_400K, xi_iC8_500K, xi_iC8_600K, and xi_iC8_700K) of the Supplementary Information (SI2.xlsx).

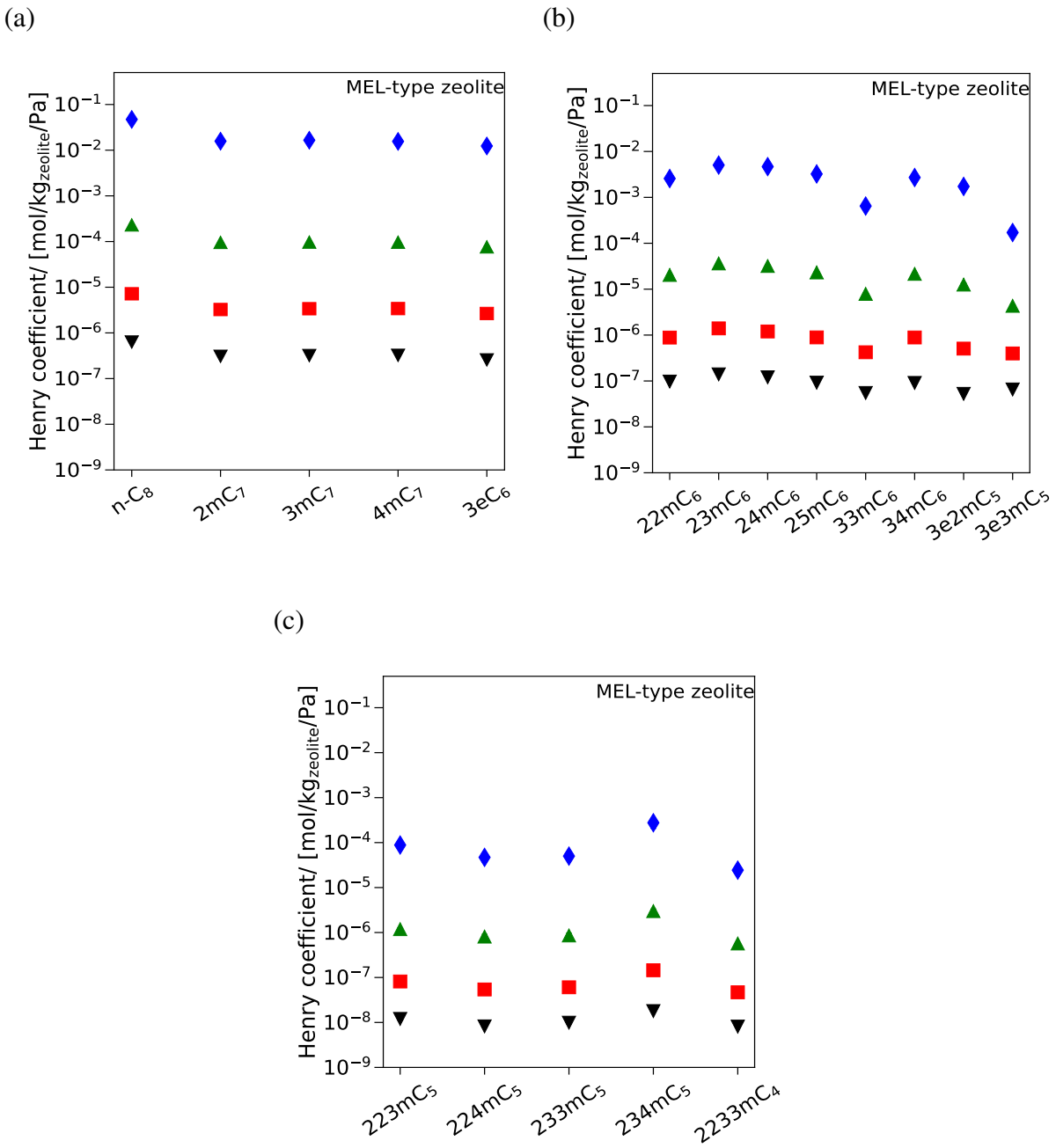

FIG. S4: Henry coefficients of C_8 isomers in MEL-type zeolite at ♦ 400 K, ▲ 500 K, ■ 600 K, and ▼ 700 K. The raw data is listed in the worksheets (xi_iC8_400K, xi_iC8_500K, xi_iC8_600K, and xi_iC8_700K) of the Supplementary Information (SI2.xlsx).

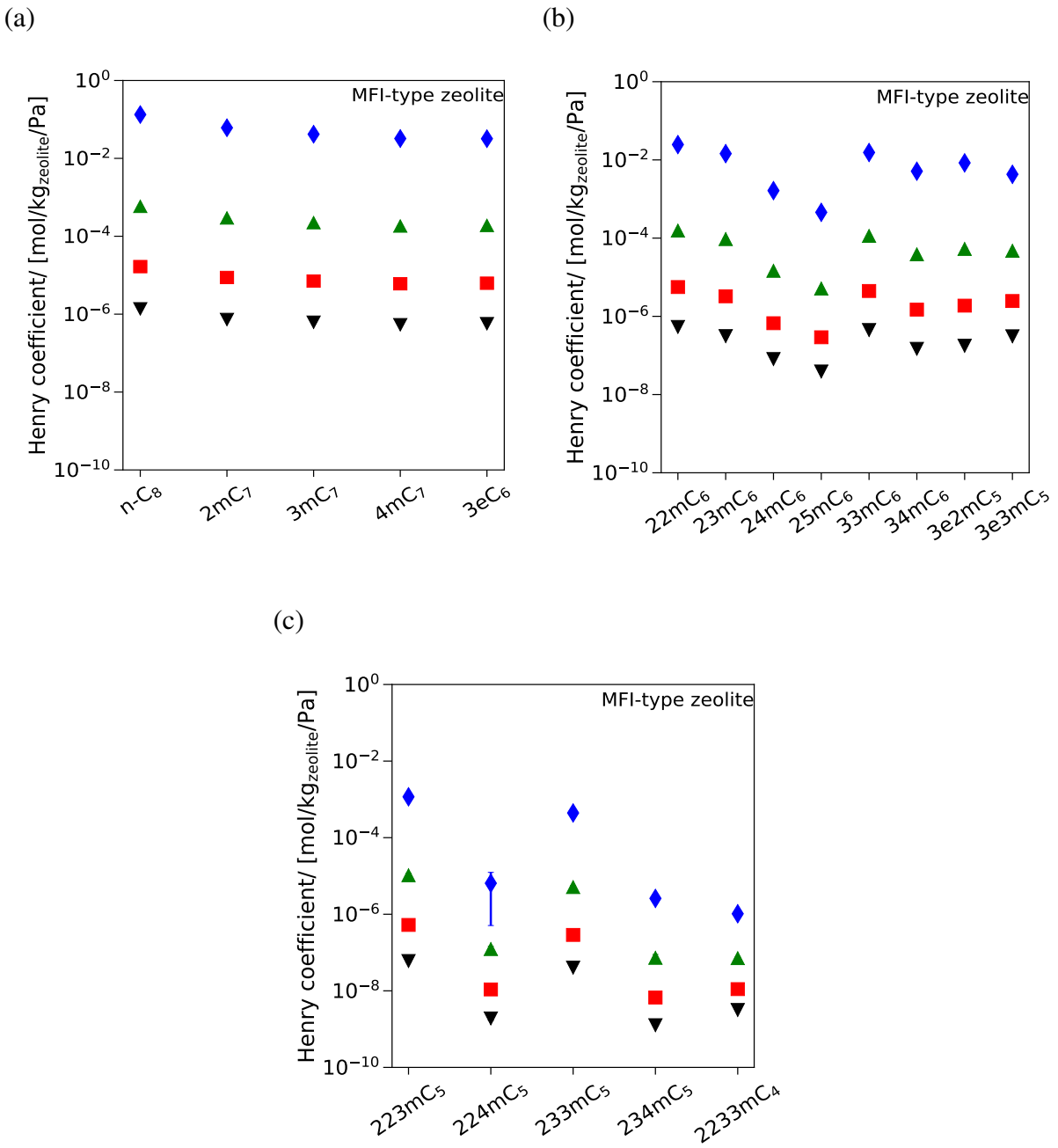

FIG. S5: Henry coefficients of C_8 isomers in MFI-type zeolite at ♦ 400 K, ▲ 500 K, ■ 600 K, and ▼ 700 K. The raw data is listed in the worksheets (xi_iC8_400K, xi_iC8_500K, xi_iC8_600K, and xi_iC8_700K) of the Supplementary Information (SI2.xlsx).

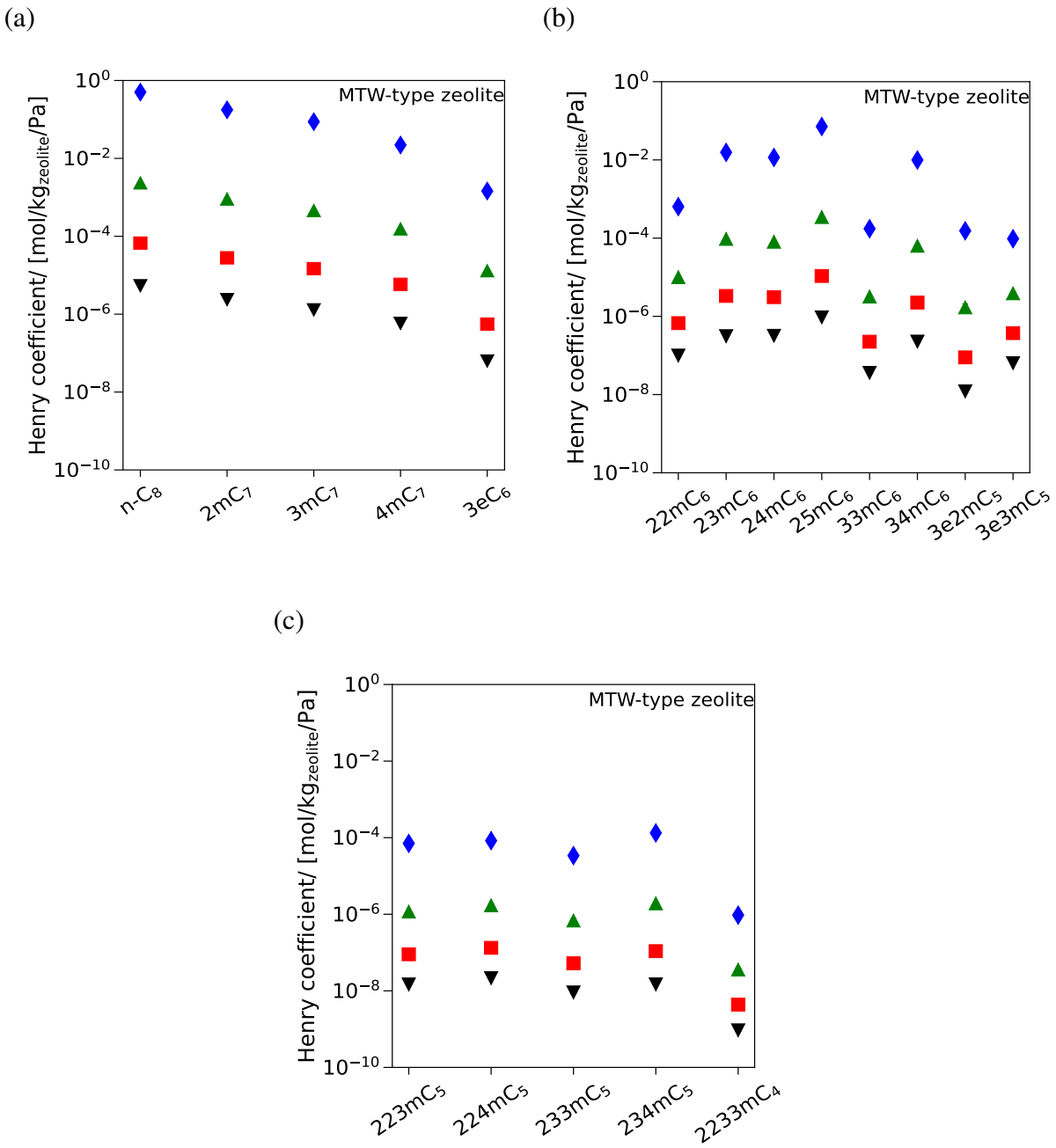

FIG. S6: Henry coefficients of C_8 isomers in MTW-type zeolite at ♦ 400 K, ▲ 500 K, ■ 600 K, and ▼ 700 K. The raw data is listed in the worksheets (xi_iC8_400K, xi_iC8_500K, xi_iC8_600K, and xi_iC8_700K) of the Supplementary Information (SI2.xlsx).

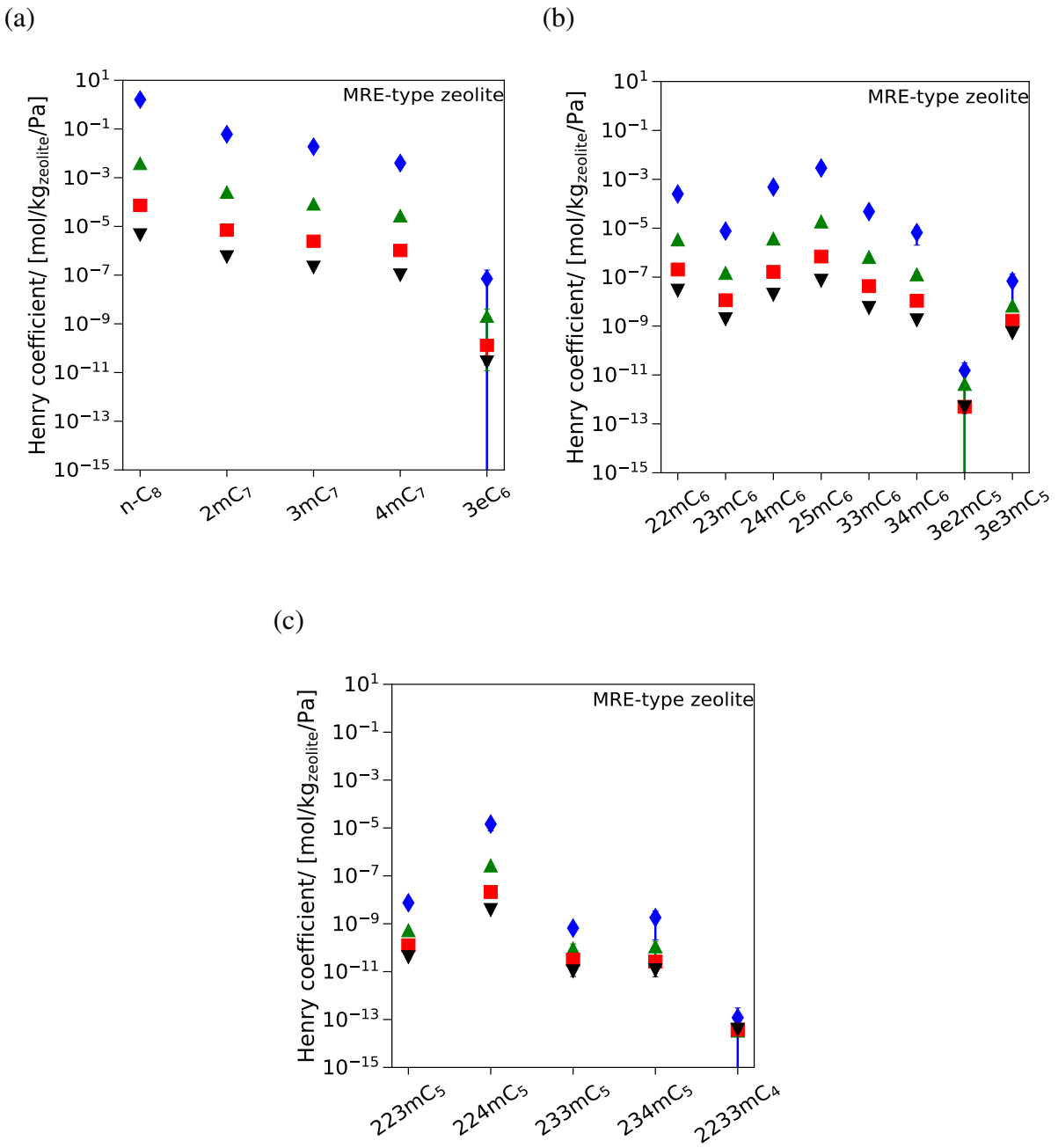

FIG. S7: Henry coefficients of C_8 isomers in MRE-type zeolite at ♦ 400 K, ▲ 500 K, ■ 600 K, and ▼ 700 K. The raw data is listed in the worksheets (xi_iC8_400K, xi_iC8_500K, xi_iC8_600K, and xi_iC8_700K) of the Supplementary Information (SI2.xlsx).

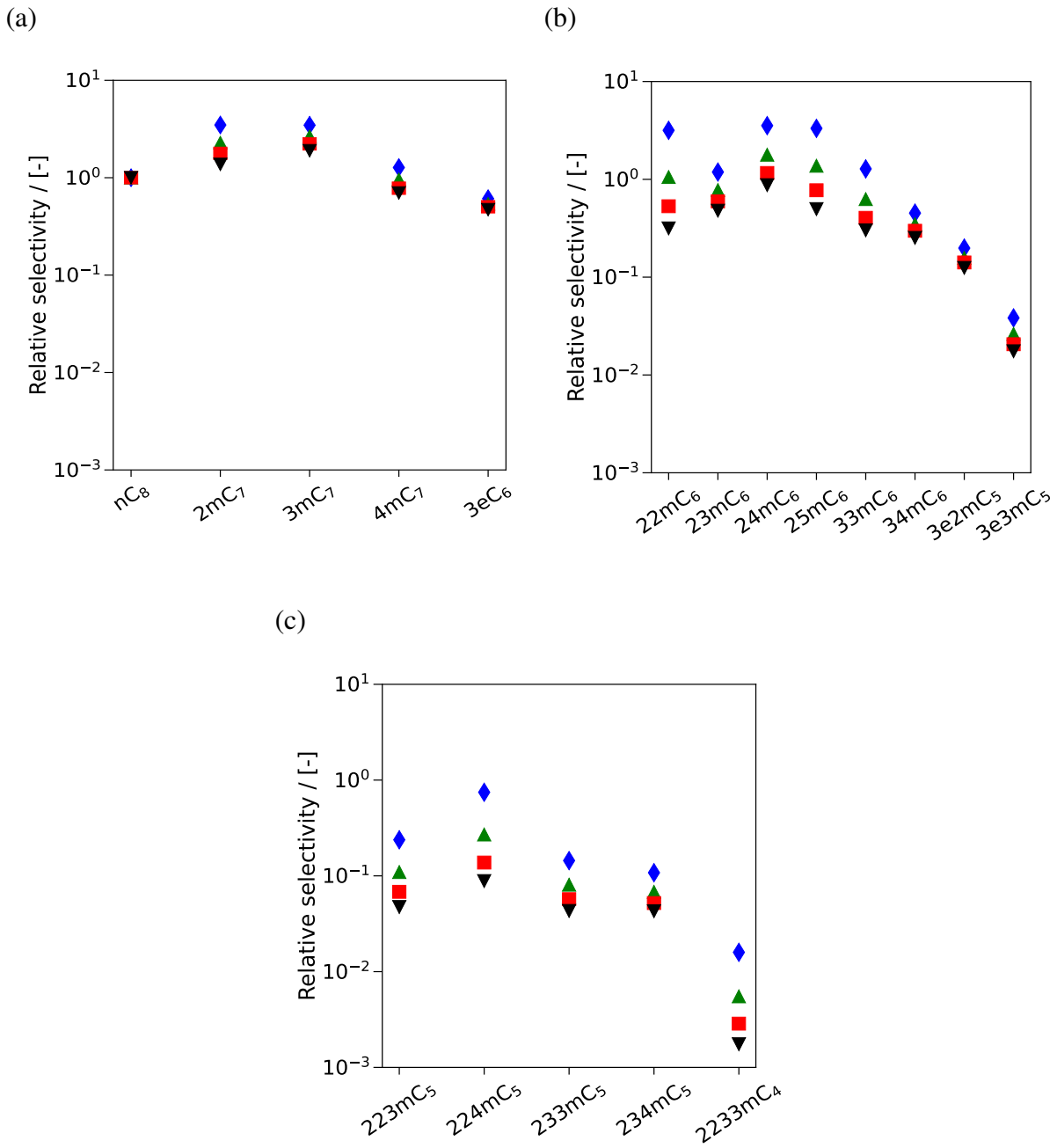

FIG. S8: Selectivities of C_8 isomers relative to n-C_8 at reaction equilibrium in the gas phase at infinite dilution. The reaction equilibrium distribution is computed at ♦ 400 K, ▲ 500 K, ■ 600 K, and ▼ 700 K. The raw data is listed in the worksheet (lnq_iC8) of the Supplementary Information (SI2.xlsx).

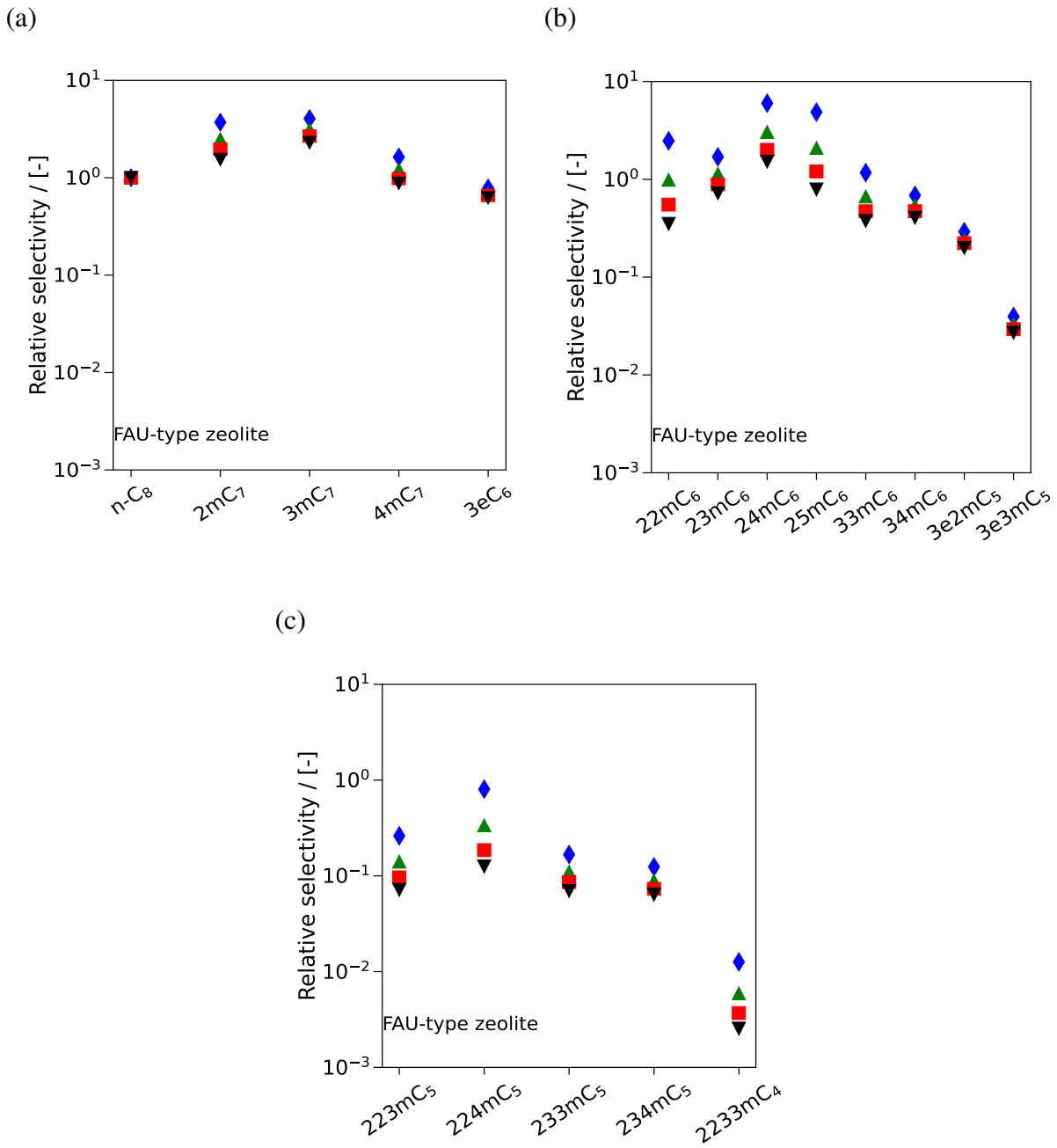

FIG. S9: Selectivities of C_8 isomers relative to n-C_8 at reaction equilibrium in FAU-type zeolite at infinite dilution. The reaction equilibrium distribution is computed at ♦ 400 K, ▲ 500 K, ■ 600 K, and ▼ 700 K. The raw data is listed in the worksheets (xi_iC8_400K, xi_iC8_500K, xi_iC8_600K, and xi_iC8_700K) of the Supplementary Information (SI2.xlsx).

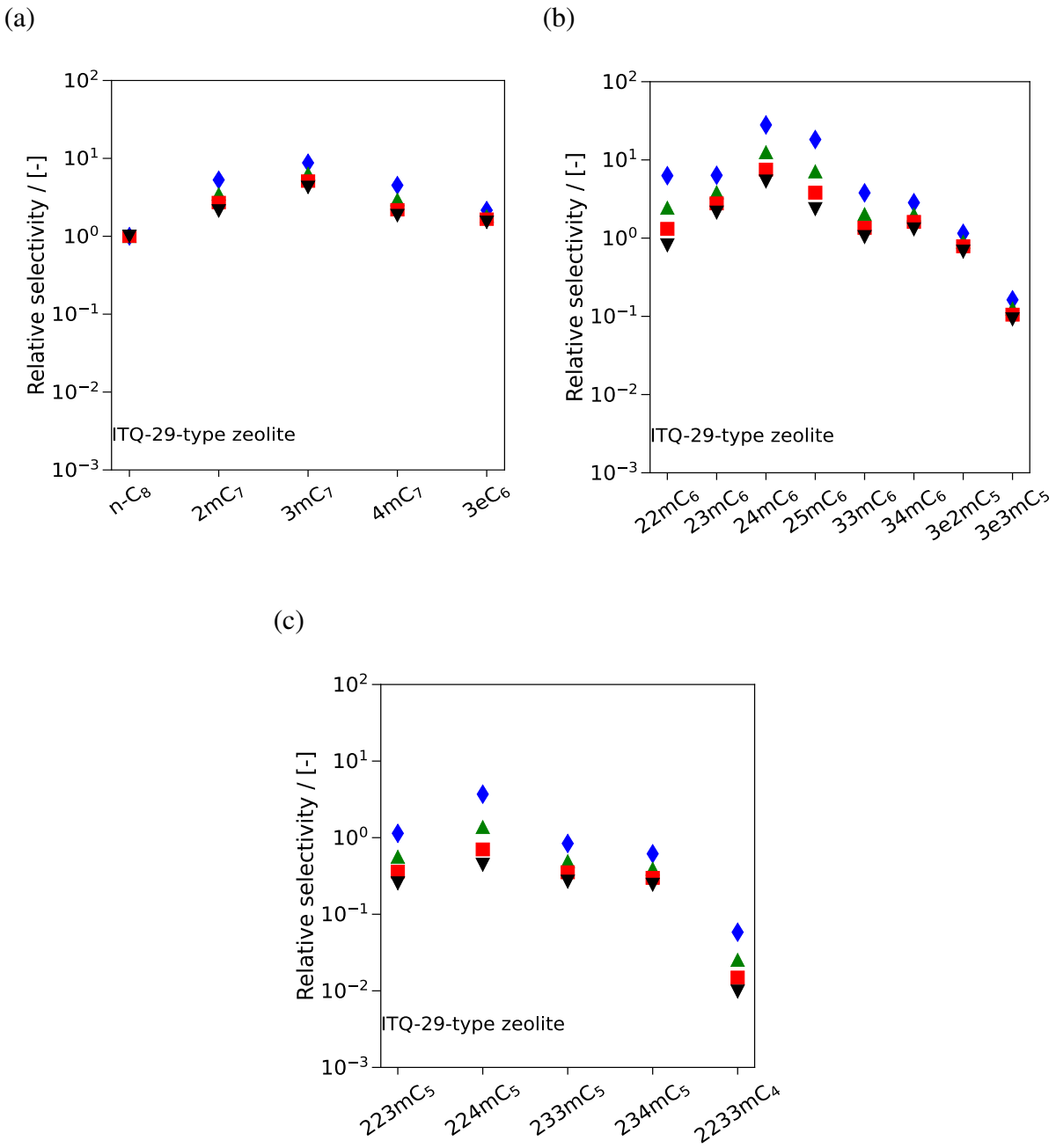

FIG. S10: Selectivities of C_8 isomers relative to n-C_8 at reaction equilibrium in ITQ-29-type zeolite at infinite dilution. The reaction equilibrium distribution is computed at ♦ 400 K, ▲ 500 K, ■ 600 K, and ▼ 700 K. The raw data is listed in the worksheets (xi_iC8_400K, xi_iC8_500K, xi_iC8_600K, and xi_iC8_700K) of the Supplementary Information (SI2.xlsx).

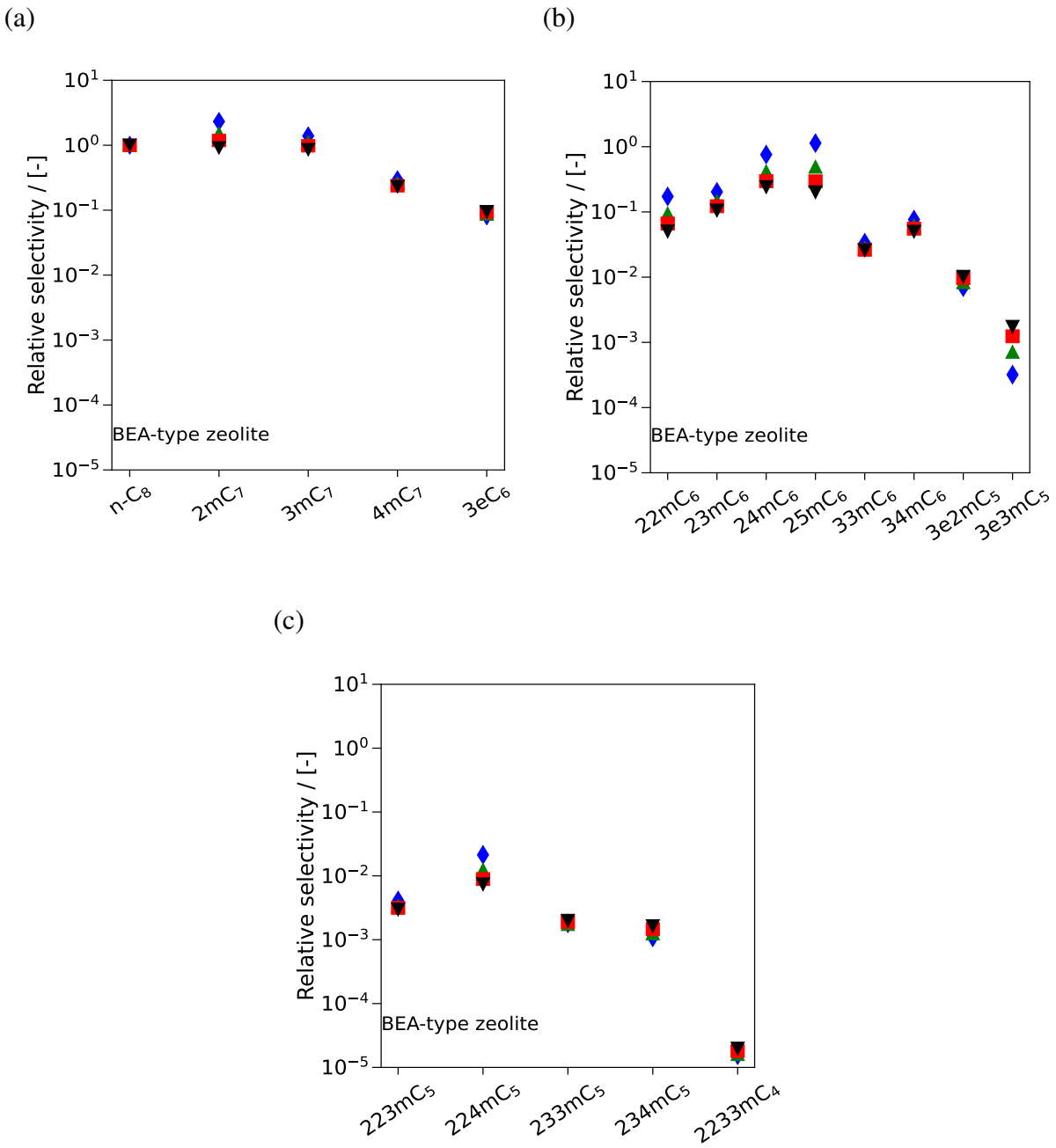

FIG. S11: Selectivities of C_8 isomers relative to n-C_8 at reaction equilibrium in BEA-type zeolite at infinite dilution. The reaction equilibrium distribution is computed at ♦ 400 K, ▲ 500 K, ■ 600 K, and ▼ 700 K. The raw data is listed in the worksheets (xi_iC8_400K, xi_iC8_500K, xi_iC8_600K, and xi_iC8_700K) of the Supplementary Information (SI2.xlsx).

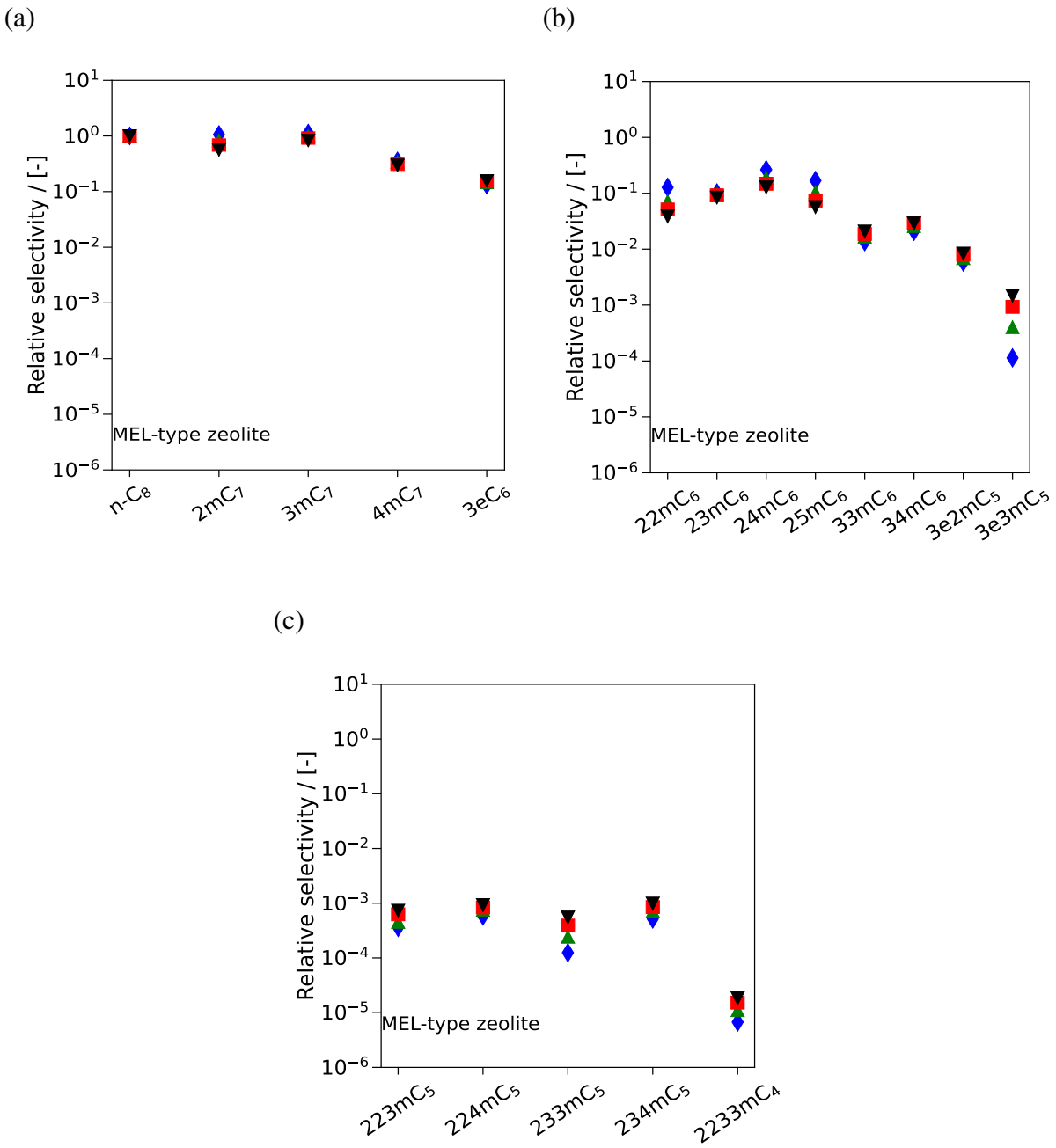

FIG. S12: Selectivities of C_8 isomers relative to n-C_8 at reaction equilibrium in MEL-type zeolite at infinite dilution. The reaction equilibrium distribution is computed at ♦ 400 K, ▲ 500 K, ■ 600 K, and ▼ 700 K. The raw data is listed in the worksheets (xi_iC8_400K, xi_iC8_500K, xi_iC8_600K, and xi_iC8_700K) of the Supplementary Information (SI2.xlsx).

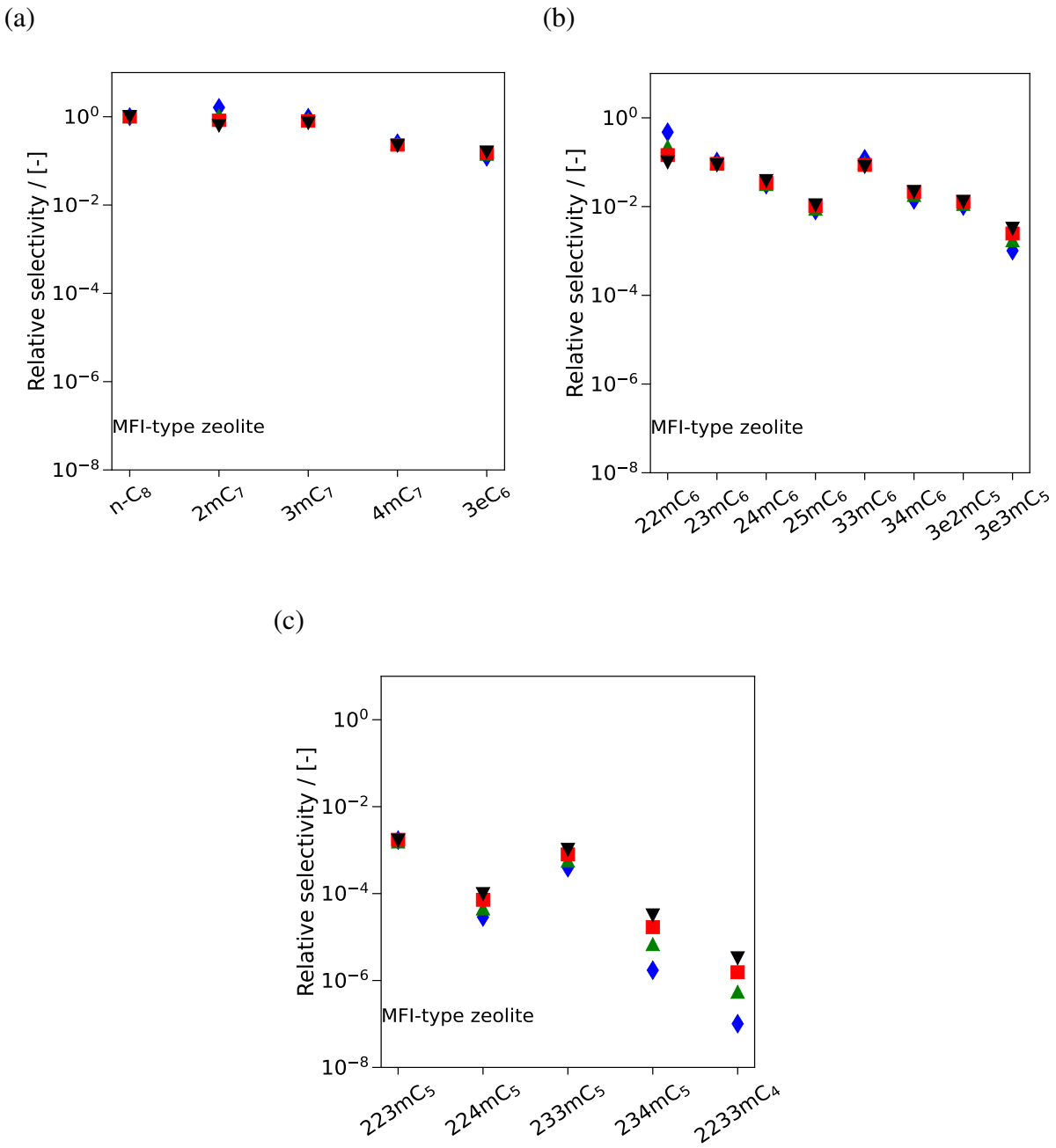

FIG. S13: Selectivities of C_8 isomers relative to n-C_8 at reaction equilibrium in MFI-type zeolite at infinite dilution. The reaction equilibrium distribution is computed at ♦ 400 K, ▲ 500 K, ■ 600 K, and ▼ 700 K. The raw data is listed in the worksheets (xi_iC8_400K, xi_iC8_500K, xi_iC8_600K, and xi_iC8_700K) of the Supplementary Information (SI2.xlsx).

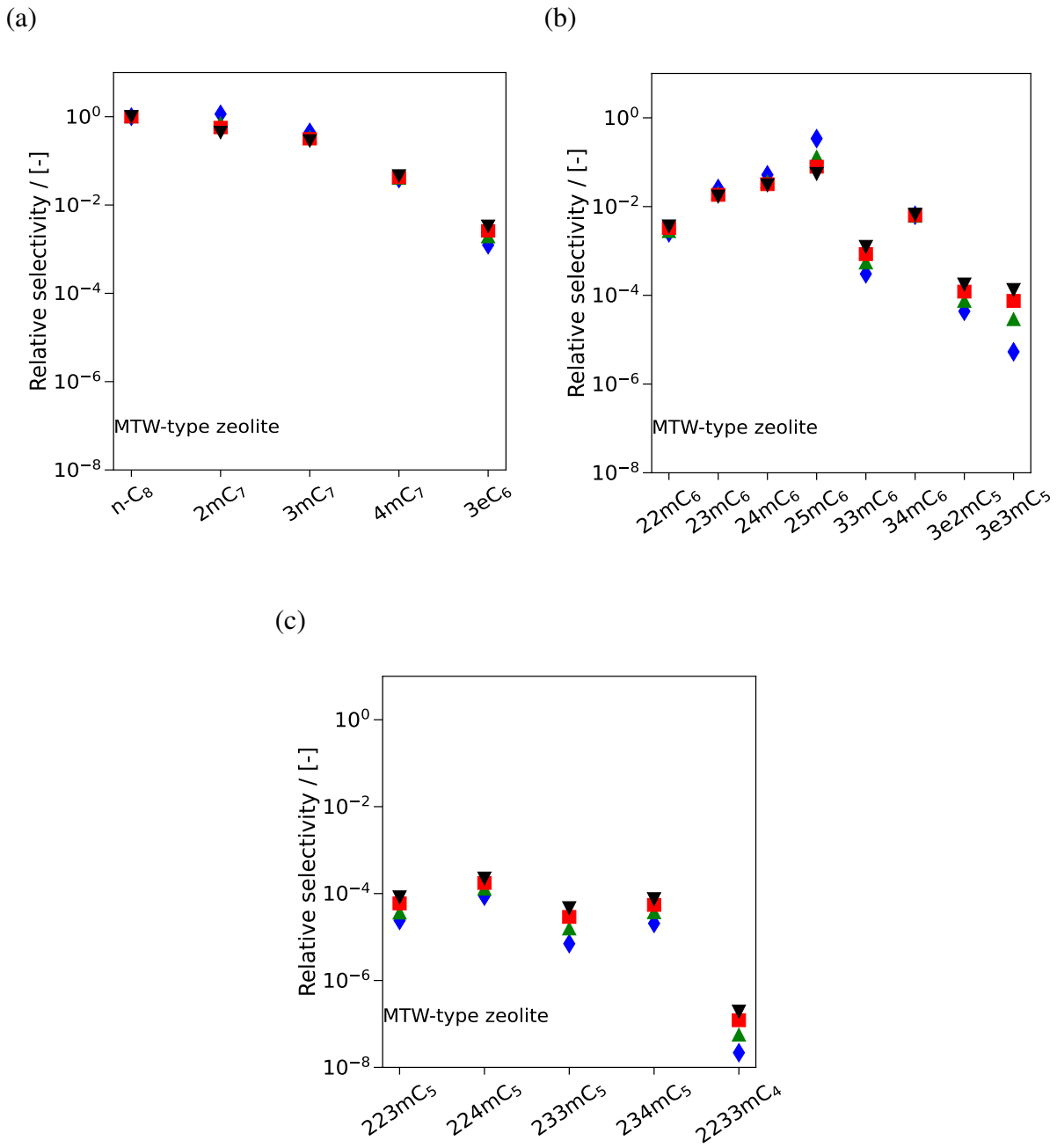

FIG. S14: Selectivities of C_8 isomers relative to n-C_8 at reaction equilibrium in MTW-type zeolite at infinite dilution. The reaction equilibrium distribution is computed at ♦ 400 K, ▲ 500 K, ■ 600 K, and ▼ 700 K. The raw data is listed in the worksheets (xi_iC8_400K, xi_iC8_500K, xi_iC8_600K, and xi_iC8_700K) of the Supplementary Information (SI2.xlsx).

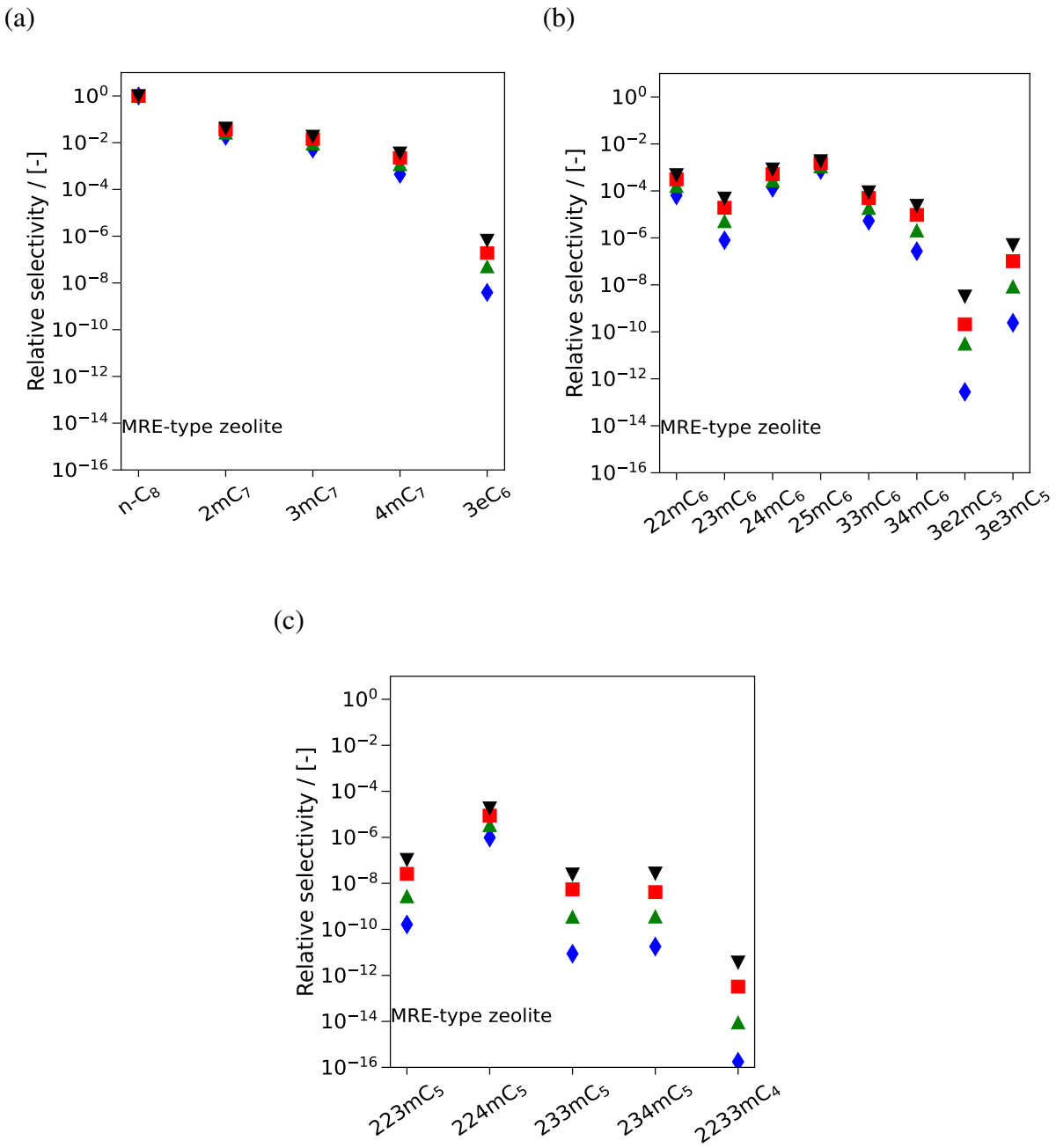

FIG. S15: Selectivities of C_8 isomers relative to n-C_8 at reaction equilibrium in MRE-type zeolite at infinite dilution. The reaction equilibrium distribution is computed at ♦ 400 K, ▲ 500 K, ■ 600 K, and ▼ 700 K. The raw data is listed in the worksheets (xi_iC8_400K, xi_iC8_500K, xi_iC8_600K, and xi_iC8_700K) of the Supplementary Information (SI2.xlsx).

[1]D. W. Scott, *Chemical thermodynamic properties of hydrocarbons and related substances: properties of the alkane hydrocarbons,* C_1 *through* C_{10}*, in the ideal gas state from 0 to 1500 K*, 1st ed. (US Department of the Interior, Bureau of Mines, Washington DC, 1974).

[2]D. Dubbeldam, S. Calero, T. J. H. Vlugt, R. Krishna, T. L. M. Maesen, and B. Smit, "United atom force field for alkanes in nanoporous materials," Journal of Physical Chemistry B **108**, 12301–12313 (2004).

[3]P. Bai, M. Tsapatsis, and J. I. Siepmann, "Trappe-zeo: Transferable potentials for phase equilibria force field for all-silica zeolites," Journal of Physical Chemistry C **117**, 24375–24387 (2013).

[4]M. P. Allen and D. J. Tildesley, *Computer simulation of liquids*, 2nd ed. (Oxford University Press, Oxford, 2017).

[5]E. G. Lewars, *Computational Chemistry. Introduction to the Theory and Applications of Molecular and Quantum Mechanics*, 2nd ed. (Springer, New York, 2011).

[6]M. G. Martin and J. I. Siepmann, "Transferable potentials for phase equilibria. 1. United-atom description of n-alkanes," Journal of Physical Chemistry B **102**, 2569–2577 (1998).

[7]C. Baerlocher, L. B. McCusker, and D. H. Olson, *Atlas of zeolite framework types*, 6th ed. (Elsevier, Amsterdam, 2007).

[8]P. Bai, M. Y. Jeon, L. Ren, C. Knight, M. W. Deem, M. Tsapatsis, and J. I. Siepmann, "Discovery of optimal zeolites for challenging separations and chemical transformations using predictive materials modeling," Nature communications **6**, 5912 (2015).

[9]O. Levenspiel, *Chemical Reaction Engineering*, 3rd ed. (John Wiley & Sons, New York, 1998).